Published in final edited form as:
Acad Radiol. 2013 August ; 20(8): 930–938. doi:10.1016/j.acra.2013.03.011.

Characterization of Texture Features of Bladder Carcinoma and the Bladder Wall on MRI:

Initial Experience

Zhengxing Shi, MS, **Zengyue Yang, MD**, **Guopeng Zhang, MS**, **Guangbin Cui, MD**, **Xiaoshuang Xiong, MS**, **Zhengrong Liang, PhD**, and **Hongbing Lu, PhD**
Department of Biomedical Engineering, Fourth Military Medical University, Xi'an, 710032, China (Z.S., G.Z., H.L.); Urology Department, Tangdu Hospital, Fourth Military Medical University, Xi'an, 710038, China (Z.Y.); Radiology Department, Tangdu Hospital, Fourth Military Medical University, Xi'an, 710038, China (G.C., X.X.); and Radiology Department, State University of New York, Stony Brook, NY (Z.L.)

Abstract

Rationale and Objectives—The purpose of this study was to determine textural features that show a significant difference between carcinomatous tissue and the bladder wall on magnetic resonance imaging (MRI) and explore the feasibility of using them to differentiate malignancy from the normal bladder wall as an initial step for establishing MRI as a screening modality for the noninvasive diagnosis of bladder cancer.

Materials and Methods—Regions of interest (ROIs) were manually placed on foci of bladder cancer and uninvolved bladder wall in 22 patients and on the normal bladder wall of 23 volunteers to calculate 40 known textural features. Statistical analysis was applied to determine the difference in these features in bladder cancer versus uninvolved bladder wall versus normal bladder wall of volunteers. The significantly different features were then analyzed using a support vector machine (SVM) classifier to determine their accuracy in differentiating malignancy from the bladder wall.

Results—Thirty-three of 40 features show significant differences between bladder cancer and the bladder wall. Nine of 40 features were significantly different in uninvolved bladder wall of patients versus normal bladder wall of volunteers. Further study indicates that seven of these 33 features were significantly different between uninvolved bladder wall of patients with early cancer and that of volunteers, whereas 15 of 33 features were different between that of patients with advanced cancer and normal wall. With the testing dataset consisting of ROIs acquired from patients, the classification accuracy using 33 textural features fed into the SVM classifier was 86.97%.

Conclusion—The initial experience demonstrates that texture features are sensitive to reveal the differences between bladder cancer and the bladder wall on MRI. The different features can be used to develop a computer-aided system for the evaluation of the entire bladder wall.

Keywords

Texture analysis; bladder cancer; computer assisted diagnosis; imaging technology-MR image

Address correspondence to: H.L. luhb@fmmu.edu.cn.
Z.S. and Z.Y. are co-first authors.

Bladder cancer is the fourth most common malignancy and accounts for 7% of all malignancies in men in the United States (1,2). In addition, according to the National Cancer Institute's Surveillance Epidemiology and End Result Registry, there has been a rising trend in bladder cancer incidence by approximately 40% since 1975 (3). In China, bladder cancer is the ninth most common malignancy in men, with increasing incidence in areas with growing aging population or the worsening environment (4,5).

The recurrence of bladder cancer is very high and even early-stage bladder cancer is likely to recur. It is estimated that 50–70% of all diagnosed cases will recur and 10–30% will progress to muscularis invasive disease (6). For this reason, bladder cancer posses a significant economic burden, and survivors often undergo follow-up tests to look for bladder cancer recurrence for years after treatment. Therefore, early detection of bladder abnormalities in high-risk populations and an appropriate follow-up procedure for survivors in a convenient and noninvasive manner is crucial to prevent the disease and reduce the death rate.

With recent advances in imaging and visualization techniques, image-based virtual cystoscopy (VCy), which involves three-dimensional surface model generation and depiction of urinary bladder based on volumetric computed tomography (CT) or magnetic resonance imaging (MRI) data, has revealed its potentials in the visualization of the mucosa layer, the evaluation of urethral orifice, and in patients with urethral stricture disease (7,8,22). Currently, most VCy systems only provide three-dimensional visualization of the entire inner surface of the bladder accompanied with two-dimensional transectional images for physician's review. Essential information, such as the detection of abnormalities, degree of muscle invasion, and staging, which is imperative for accurate diagnosis and treatment planning of invasive bladder cancer, could not be obtained directly in VCy, limiting its further use in bladder surveillance.

As reported, bladder carcinoma invades gradually from the mucosa into the wall muscles and is categorized into different stages (2,3). Imaging is an essential part of clinical staging. Several recent studies have shown that geometric analysis and intensity features of the bladder wall tend to be good indicators for the occurrence of abnormalities. Especially, textural features that reflect intensity variation and tissue patterns have the potential to differentiate carcinomatous tissues from normal tissues and reflect the transition of different stages (9,10,17,22). For example, Sheshadri et al. used texture features from mammograms to classify different types of breast tissues, which led to a new method for early detection of breast cancer (9). Ganeshan et al. concluded that texture analysis in noncontrast-enhanced CT could reflect changes in disease-free areas of the liver (10). Nailon et al. reported three texture features that were sensitive to differentiate bladder, rectum, and perivesical tissues on CT images (17). Based on these observations, it is hypothesized that if characteristic texture features that could differentiate bladder cancer from normal tissues are available, they may help us to detect the abnormalities in an automatic way, ie, computer-aided detection (CAD), and furthermore to help determine the invasion stage of bladder cancer into the bladder wall muscle, ie, computer aided diagnosis (CADx).

Though both CT and MRI are clinically used for bladder imaging, the MRI modality has more advantages because of its noninvasive and radiation-free nature as well as its high intensity-contrast between the bladder neoplasm, the bladder wall, and urine exhibited on specific MRI sequences. Previous studies have shown a superior accuracy of MRI in detecting the local staging of bladder tumors and in predicting the wall and perivesical infiltration (11). The purpose of this study was to determine features that show a significant difference between carcinomatous tissue and the bladder wall on MRI and explore the feasibility of using them to differentiate malignancy from the normal bladder wall as an

initial step for CAD of tumor detection. It is also an essential step forward to establishing MRI as a screening modality for the noninvasive diagnosis of bladder cancer.

MATERIALS AND METHODS

Subjects

Twenty-two consecutive male patients in whom findings from routine cystoscopy were positive for tumors were referred from the urology department, Tangdu Hospital, Xi'an, China, between March 2008 and May 2010. All the patients were confirmed of having urothelial carcinoma by postoperative pathological biopsy. Twenty-three male volunteers were also recruited simultaneously as the control group; they had no known history of bladder diseases, no bladder mass observed during the ultrasound examination, and no hematuria. The research trial has been approved by the Hospital Ethics Committee and informed written consent was obtained from each patient and volunteer.

Imaging Protocols

Though gadolinium-enhanced MRI has shown better staging accuracy in some studies (6), a protocol without contrast enhancement would be more acceptable for routine check or mass screening. To find a protocol that better accommodated to this study, several T_2-weighted sequences that exhibit high contrast between the bladder wall and urine, including a free breathing T_2-weighted fast spin-echo, a free breathing T_2-weighted single-shot fast spin-echo (SSFSE), and a T_2-weighted fast spin-echo respiratory trigger sequence, were tested on both patients and volunteers, respectively. Finally the T_2-weighted SSFSE was selected because it is less susceptible to motion than other sequences and is a fast sequence that is more acceptable for volunteer scans.

All MRI examinations in this study were performed by a 3.0 T scanner (MR-Signa EXCITE HD, GE) with a phased-array abdominal/pelvis coil (TORSOPA, GE). Before the examination, each subject (patient or volunteer) was asked to drink enough mineral water and then wait for an adequate time period so that the bladder was distended sufficiently. An axial T_2-weight SSFSE sequence was performed with the following parameters of repetition time/echo time: 2117.6/78.0 ms, matrix: 512 × 512, field of view: 40 cm, thickness: 3.0 mm, and intersection gap: 0.5 mm. The acquisition time was 67–102 seconds for each plane. Sagittal or coronal T_2-weighted images were added if the tumor was located in the base or the dome of the bladder. No contrast agent was used and all the subjects were examined in supine position.

ROI Measurements

To identify characteristic image features that could reflect the difference between malignancy and the bladder wall, regions of interest (ROIs) were first manually placed on foci of bladder cancer and uninvolved bladder wall in 22 patients and on normal bladder wall of 23 volunteers. All borders of the ROIs were carefully traced so that only one type of tissue was encircled in one ROI, as shown in Figure 1. Considering the invasive nature of tumors, the bladder wall ROI of each patient was placed with a certain distance away from the tumor boundary. To ensure correct enclosure of carcinoma or bladder wall tissues, all ROIs were first placed using a self-developed software package by two experienced radiologists with reading experience of more than 10 years. The third radiologist with reading experience of more than 20 years made a final decision for each ROI based on their results (Fig 1).

For later statistical analysis, all ROIs were divided into three groups (group A, bladder carcinoma of patients; group B, uninvolved bladder wall of patients; and group C, normal

bladder wall of volunteers). Here we separated ROIs of the bladder wall into two groups (B and C) to explore whether the image pattern of patients' bladder wall the same as that of volunteers'.

Texture Analysis

Based on extracted ROIs, statistical analysis on texture features among the three groups was performed with two steps below: 1) extracting texture features from each ROI and 2) performing statistical analysis on extracted features.

In the first step, both statistical-based and structural-based features could be used for textural analysis. Considering the relatively poor pattern regularity and fine textures exhibited in medical images, only statistical-based textural features that have been reported in previous publications were compared in this study. Finally, five categories of texture features were extracted from each ROI to explore textural characteristics of different types of tissues, including: 1) features based on the probability distribution of image intensity in each ROI, including mean, entropy, uniformity, smoothness, standard deviation (SD), skewness, third moment (Tm), and kurtosis (9,10) (eight features); 2) features based on auto-covariance coefficients (Cov), ie, norm of vector (Norm) (12); 3) textural features related to visual perception that are called Tamura features, including contrast, directionality, line-likeness, and regularity (13) (four features); 4) textural features derived from the gray level cooccurrence matrix (GLCM), where each element represents the relative frequency with which two pixels with given gray levels are separated by a given pixel distance. Considering that the bladder wall is relatively thin, a fixed distance was used for the calculation of GLCM, and a total of 16 features were derived (f1–f16) (14,15); and 5) textural features derived from the gray level-gradient co-occurrence matrix (GLGCM) that reflects the spatial variation of gray level and gradient. For similar reason, a fixed pixel distance was considered and a total of 11 features were calculated (T1–T11) (16). Taken together, 40 features were extracted from each ROI for further analysis. Tables 1a and 1b provide information on these textural features.

Most of the 40 features were designed for regularly shaped ROIs in previous studies. In this study, however, nearly all ROIs were irregular, including long and narrow ones from the bladder wall. For accurate feature calculation, some modifications were applied for irregularly shaped ROIs. In particular, when the calculation involved in pixels located at the ROI boundary or neighboring pixels outside the ROI (background pixels), the average intensity of non-background pixels inside the 3 × 3 neighborhood of the pixel would be used. In addition, if the number of nonbackground pixels inside the neighborhood was less than a preset threshold (depending on feature types), the pixel would not be considered in the calculation any more. For simplicity, all features were calculated in two-dimensional by a locally developed software package using Matlab7.6.

In the second step, sample *t*-test and the variance analysis (one-way analysis of variance) were applied to multiple features to evaluate the significance of difference among the three groups (ie, group A, carcinoma tissues of patients; group B, uninvolved bladder wall of patients; and group C, normal bladder wall of volunteers). The results were expressed as mean absolute deviations between these groups. The significance threshold was set as $P < .01$ and all the statistical analysis was performed by the SPSS12.0 package.

Initial Classification Using Selected Features

To test the feasibility of using statistically significant features for the differentiation of malignancy from the bladder wall, initial classification study was further performed. Considering its generalization capability and high performance, a classical support vector

machine classifier was employed, with the radial basis function as the kernel function. Significantly different features were fed into the classifier to determine their accuracy in differentiating malignancy from the bladder wall. To train and test the classifier with limited amount of ROI data, leave-one-out cross-validation was used. All feature vectors extracted from ROIs of patients, including both groups A and B, were randomly divided into 10 subsets. The classifier was trained by nine subsets and tested by the left. The process was repeated 10 times so that each subset was used once as the testing data. The performance of the classifier was evaluated as the average of the accuracy rates of 10 times.

RESULTS

Table 2 shows the age distribution, histological subtypes, and staging of all patients. The age of volunteers ranges from 28 to 64, with mean and standard deviation of 46.55 ± 13.19. There was no significant difference in age between the two groups.

Among 22 patients enrolled, all tumors were polypoidal shaped and the size of bladder tumors ranged from 0.5 to 6 cm in diameter. Because the smallest one was too small to be encircled, it was not included in group A. In addition, the bladder wall of two patients were hardly outlined because of motion artifacts and therefore not included in group B. For each dataset, about 5–20 ROIs of the bladder wall were placed depending on the number of bladder images, whereas 3–13 tumor ROIs were outlined from each patient's dataset based on the size of bladder tumor. In total, in this study, group A includes 118 tumor ROIs from 21 patients, group B includes 189 wall ROIs from 20 patients, and group C represents 142 wall ROIs from 23 volunteers.

It has been widely recognized that carcinomatous tissues (bladder cancer) and smooth muscle (bladder wall) are two different types of tissues pathologically. To see whether image features could reflect the difference, the *t*-test was first performed between the samples in groups A and B. Thirty-three of 40 features show significant difference ($P < .01$) between the two groups, as shown in Table 3, including mean, entropy, uniformity, smoothness, SD, Tm, norm, contrast, line-likeness, 14 of 16 GLCM features (f1–f16 except for f_{12}, f_{13}), and 10 of 11 GLGCM features (T1–T11 expect for T_6). The relatively high rate of 82.5% features having difference indicates that the pathological difference between the two types of tissues could be reflected by textural features. Based on this analysis, it could be postulated that these features may be further applied to differentiate malignancy from the bladder wall.

After the test between groups A and B, the *t*-test was then extended to the samples in groups B and C to explore whether the image textures of patients' bladder wall differ from those of volunteers'. Nine of 40 features show significant difference ($P < .01$) between the two groups, including 1) two intensity features (ie, entropy and uniformity), 2) one Tamura feature (ie, directionality), 3) three GLCM features (ie, f_1, f_9, and f_{12}), and 4) three GLGCM features (ie, T_5, T_6, and T_9), as shown in Table 4. Anatomically the bladder wall of both patients and volunteers was composed of smooth muscle and correspondingly the image texture would be similar. However, nine of 40 features are significantly different between them. A possible reason is that the bladder wall of patients might undergo some pathological process, which was reflected by some image features.

To see whether the variation on the bladder wall of patients correlates with cancer staging, group B was further divided into two subgroups. B_1 included samples from patients with early cancer (Ta, T1, and T2) and B_2 includes samples from patients with advanced cancer (T3 and T4). The total number of patients is 16 for B_1 and 4 for B_2 and a corresponding total number of ROIs is 135 for B_1 and 54 for B_2, respectively. The variance analysis was

performed between samples in subgroups B_1 or B_2 and samples in group C. Only 33 features that have showed significant differences in the first experiment were used in this analysis.

The analysis result shown in Table 5 indicates that seven of 33 features (ie, entropy, uniformity, Tm, T5, T9, f1, and f9), are significantly different ($P < .05$) between subgroup B_1 and group C. Meanwhile, 15 of 33 features are significantly different ($P < .05$) between subgroup B_2 and group C, including entropy, uniformity, SD, line_likeness, T_3–T_5, T_7–T_9, f_1, and f_8–f_{11}. Combining the two tables, six features (ie, entropy, uniformity, T5, T9, f1, and f9) are significantly different, not only between groups B and C, but also between groups B_1 and C and between groups B_2 and C. In addition, nine features, which are not significant between subgroups B_1 and C, show significant difference between B_2 and C. The result indicates that although bladder cancer occurs at a limited area, it may have an impact on the bladder wall. With the development of bladder cancer from early stage to advanced stage, more difference between the bladder wall of patients and normal bladder wall may be detected by texture features.

Based on the results in Tables 2–5, it can be deduced that not only the textural pattern of bladder carcinoma differs greatly from the bladder wall, but also that a difference between the bladder wall of patients with early cancer and that of patients with advanced cancer may also exist. In other words, changes of texture patterns on MRIs may reflect the existence of bladder cancer and further the staging of bladder cancer. With the integration of features reflecting the difference between carcinoma and normal wall, a CAD system for the detection and staging of bladder cancer may be possible.

To test the feasibility of using these textural features for the differentiation of malignancy from the bladder wall, the support vector machine classifier was trained and tested by the testing dataset consisting of total 307 ROIs from groups A and B. The exhaustion method was used to search for the optimal parameter combination for the classifier. Using 33 significant features shown in Table 3, the classification accuracy of 10 training and testing rounds was 86.97%. It indicates the potential of using textural features to differentiate bladder cancer from its surrounding bladder wall.

DISCUSSION

In the past few years, CAD/CADx for breast cancer, pulmonary nodules, and colon polyps has been a very active research topic, aiming to assist physicians to detect and distinguish nodules and polyps from benign to malignant. The achievement is still moderate possibly because the primary consideration of the outside characteristics on the surface of nodules or polyps. It was gradually recognized that different image textural patterns may reflect different types of tissues and can be used to distinguish carcinomatous tissues from healthy tissues on images. For clinical application on bladder evaluation, it was hypothesized that bladder carcinoma could be separated from normal wall and therefore the abnormalities and the invasion of malignancy into the muscle layers could be noninvasively recognized if the imaging modality is sensitive enough to reveal the information. The results of this study indicate that the specific MRI sequence may be sensitive enough to reveal the textural difference between bladder cancer and the bladder wall.

For noninvasive detection of bladder cancer based on MRI scans, another important issue is to find sensitive features that reflect the textural difference. Previous study performed by Nailon et al. investigated possible texture features that were sensitive to differentiate bladder, rectum, and perivesical tissues on CT images (17). In this study, we focused on the determination of textural features reflecting the difference between bladder cancer and the bladder wall. Preliminary results demonstrate that 33 of 40 features tested here could reflect

the textural difference between the two types of tissues ($P < .01$). Three features investigated by Nailon et al. were also included in this study and exhibited good sensitivity on MRI images.

Further statistical analysis on feature difference between uninvolved bladder wall of patients and normal bladder wall of volunteers indicates that nine of 40 features are significantly different ($P < .05$). It suggests that the bladder wall of patients may differ from that of healthy volunteers, which may be caused by the proliferation and invasion of cancerous tumors into the bladder wall. To further identify whether the textural pattern of the bladder wall changes with cancer staging, wall ROIs of patient were divided into two subgroups (ie, B_1 including wall ROIs from patients with early cancer and B_2 including wall ROIs from patients with advanced cancer). Although only seven of those 33 features show significant difference between B_1 and group C, 15 of 33 features show significant difference between B_2 and group C. In other words, 26 of 33 features do not differ in uninvolved bladder wall of patients with early cancer and normal bladder wall, indicating the similar pattern of their intensity distributions. However, that 15 of 33 features differs between the bladder wall of patients with advanced cancer and that of volunteers indicates possibly different patterns between the two groups. These observations are consistent with some findings published previously. For example, in 2011 National Comprehensive Cancer Network guidelines, it is claimed that bladder wall thickening suggest the presence of T3a stage of bladder cancer (18) and Jaume et al. has tried to detect bladder tumor based on abnormal thickness of bladder wall in CT scans (19). Victor's study (20) indicates that vascular invasion of bladder cancer is associated with disease progression. Some other reports further argue that the long-term recurrence of bladder cancer and treatment of drugs lead to bladder fibrosis. All these facts indicate that with the rampancy of vascular invasion and fibrosis into the bladder wall, the change of texture pattern on MRI scans may reflect the invasion of malignancy.

Further analysis on the experimental results of three groups indicates that 9 features (ie, SD, line_likeness, T_3, T_4, T_7, T_8, f_8, f_{10}, and f_{11}) were different between the bladder wall of patients with advanced cancer (subgroup B_2) and that of volunteers, but not different between patients with early cancer (subgroup B_1) and volunteers. Meanwhile, these nine features were significantly different between bladder cancer (group A) and uninvolved bladder wall of patients (group B), but not significant between the bladder wall of patients (group B) and that of volunteers (group C). It suggests that they may be the most suitable features with which to distinguish bladder carcinoma from the bladder wall, and could be used as candidates for CAD of bladder abnormalities. In addition, there are six features (ie, entropy, uniformity, T_5, T_9, f_1, and f_9) that were not only significantly different between groups B_1 and C, groups B_2 and C, but also different between groups A and B. That means these features may have the potential to reflect subtle difference on textural patterns between the bladder wall and bladder cancer, and therefore can be applied as candidates to detect bladder cancer at early stages.

As reported, clinical staging is an important yet imperfect evaluation of patients with bladder cancer, with about 30–50% of patients clinically understaged at the time of cystectomy (6), which can lead to incomplete resection and higher recurrence rates. According to the 2011 National Comprehensive Cancer Network guidelines for bladder cancer, surveillance cystoscopy and urine cytology should be performed every 3 months for patients without muscularis invasive disease for the first 1–2 years, repeated at increasing intervals over the next 2 years (18). Any unnecessary delays on treating muscularis invasive bladder cancer should be avoided because a more than 12-week delay was associated with advanced pathological stage and decreased survival (6). Therefore, noninvasive and convenient detection of bladder cancer would be critical for the management of recurrence and increased survival. With noninvasive MRI, the proposed features could be used to

differentiate bladder cancer from the bladder wall as an initial step of a CAD system for bladder cancer detection (23). Further integration of extracted features with a CADx system would make the staging of bladder cancer possible in a noninvasive and automated way, resulting in more accurate pretreatment diagnosis.

Meticulous bladder preparation and adequate distension are critical for an accurate interpretation of bladder images. Retained fluid or lack of adequate bladder distension may interfere with the correct diagnosis (21). In this study, with the proposed MRI sequence, contrast enhancement would not be necessary because of natural contrast between the bladder wall and urine. What the patients needed to do was to drink enough water and wait for the bladder to be distended sufficiently. The proposed routine for bladder cancer surveillance would be attractive to clinics and public health because of its higher acceptance by patients as well as its considerably low risk.

Though the preliminary results are promising, further investigation is needed. More patients with bladder cancer at different stages should be recruited in further study to increase the reliability of proposed textural features and to detect the invasion of bladder cancer into the bladder wall. In this study, interactive segmentation was used for correct inclusion of different types of tissues in the ROI, which was quite time-consuming. To integrate the proposed pipeline into a virtual cystoscopy system for clinical screening, automatic segmentation of carcinoma and the bladder wall should be required. Developing a CAD/CADx system for virtual cystoscopy based on MRI scans is our ultimate goal, which will provide an objective and consistent tool for fast evaluation of the entire bladder.

Acknowledgments

This work was partially supported by the National Nature Science Foundation of China under grants 81230035 and 81071220. Zhengrong Liang was partially supported by National Institute of Health grant #CA082402.

References

1. American Cancer Society. Cancer facts & figures 2012. Atlanta (GA): American Cancer Society; 2012.
2. Kirkali Z, Chan T, Murugesan M, et al. Bladder cancer: epidemiology, staging and grading, and diagnosis. Urology. 2005; 66(Suppl 6A):4–34. [PubMed: 16399414]
3. Bladder Cancer Clinical Guideline Update Panel. Bladder cancer: guideline for the management of nonmuscle invasive bladder cancer: (stages Ta, T1, and Tis): 2007 update. Linthicum, MD: American Urological Association; 2007.
4. Chinese diagnosis and treatment guidelines in urology surgery. China Urology Surgery Society; 2007. Committee of Chinese diagnosis and treatment guidelines in urology surgery.
5. [Accessed April 15, 2012] The top ten malignancy mortality rates of China (man) [EB/OL]. Available at: http://61.49.18.65/htmlfiles/zwgkzt/ptjnj/year2010/index2010.html
6. Jacobs BL, Lee CT, Montie JE. Bladder cancer in 2010: how far have we come? CA Cancer J Clin. 2010; 60:244–272. [PubMed: 20566675]
7. Kim JK, Ahn JH, Park T, et al. Virtual cystoscopy of the contrast material-filled bladder in patients with gross hematuria. AJR Am J Roentgenol. 2002; 179:763–768. [PubMed: 12185059]
8. Arslan H, Ceylan K, Harman M, et al. Virtual computed tomography cystoscopy in bladder pathologies. Clin Urol. 2006; 32:147–154.
9. Sheshadri HS, Kandaswamy A. Experimental investigation on breast tissue classification based on statistical feature extraction of mammograms. Comp Med Imaging Graphics. 2007; 31:46–48.
10. Ganeshan B, Miles KA, Young RC, et al. Texture analysis in non-contrast enhanced CT: impact of malignancy on texture in apparently disease-free areas of the liver. Eur J Radiol. 2009; 70:101–110. [PubMed: 18242909]

11. Totaro A, Pinto F, Brescia A, et al. Imaging in bladder cancer: present role and future perspectives. Urol Int. 2010; 85:373–380. [PubMed: 20962513]
12. Wu W-J, Moon WK. Ultrasound breast tumor image computer-aided diagnosis with texture and morphological features. Acad Radiol. 2008; 15:873–880. [PubMed: 18572123]
13. Tamura H, Mori S, Yamawaki T. Textural features corresponding to visual perception. IEEE Trans Syst Man Cybernetics. 1978; 8:460–473.
14. Robert MH, Shanmugam K, Dinstein I. Textural features for image classification. IEEE Trans Syst Man Cybernetics. 1973; SMC-3:610–621.
15. Conners RW, Trivedi MM, Harlow CA. Segmentation of a high-resolution urban scene using texture operators. Comp Vision Graphics Image Pro. 1984; 25:273–310.
16. Scher A, Rosenfeld A. "Probability transforms" of digital pictures. Pattern Recognit. 1980; 12:457–468.
17. Nailon, WH.; Redpath, AT.; McLaren, DB. Texture analysis of 3D bladder cancer CT images for improving radiotherapy planning. Paris, France. 13th International Power Electronics and Motion Control Conference; 2008. p. 652-655.
18. National Comprehensive Cancer Network. NCCN Clinical Practice Guidelines in Oncology: Bladder Cancer VII. Vol. 2011. National Comprehensive Cancer Network; 2011.
19. Jaume S, Ferrant M, Macq B, et al. Tumor detection in the bladder wall with a measurement of abnormal thickness in CT scans. IEEE Trans Biomed Eng. 2003; 50:383–390. [PubMed: 12669995]
20. Reuter VE. The pathology of bladder cancer. Urology. 2006; 67:11–18. [PubMed: 16530068]
21. Lämmle M, Beer A, Settles M, et al. Reliability of MR imaging-based virtual cystoscopy in the diagnosis of cancer of the urinary bladder. AJR Am J Roentgenol. 2002; 178:1483–1488. [PubMed: 12034625]
22. Bernhardt TM, Schmidl H, Philipp C, et al. Diagnostic potential of virtual cystoscopy of the bladder: MRI vs. CT – preliminary report. Eur Radiol. 2003; 13:305–312. [PubMed: 12598995]
23. Shi Z, Lu H, Wu Z, et al. Computer-aid detection and stage assessment of bladder cancer based on MR image. Int J CARS. 2012; 7(Suppl):S275–S277.

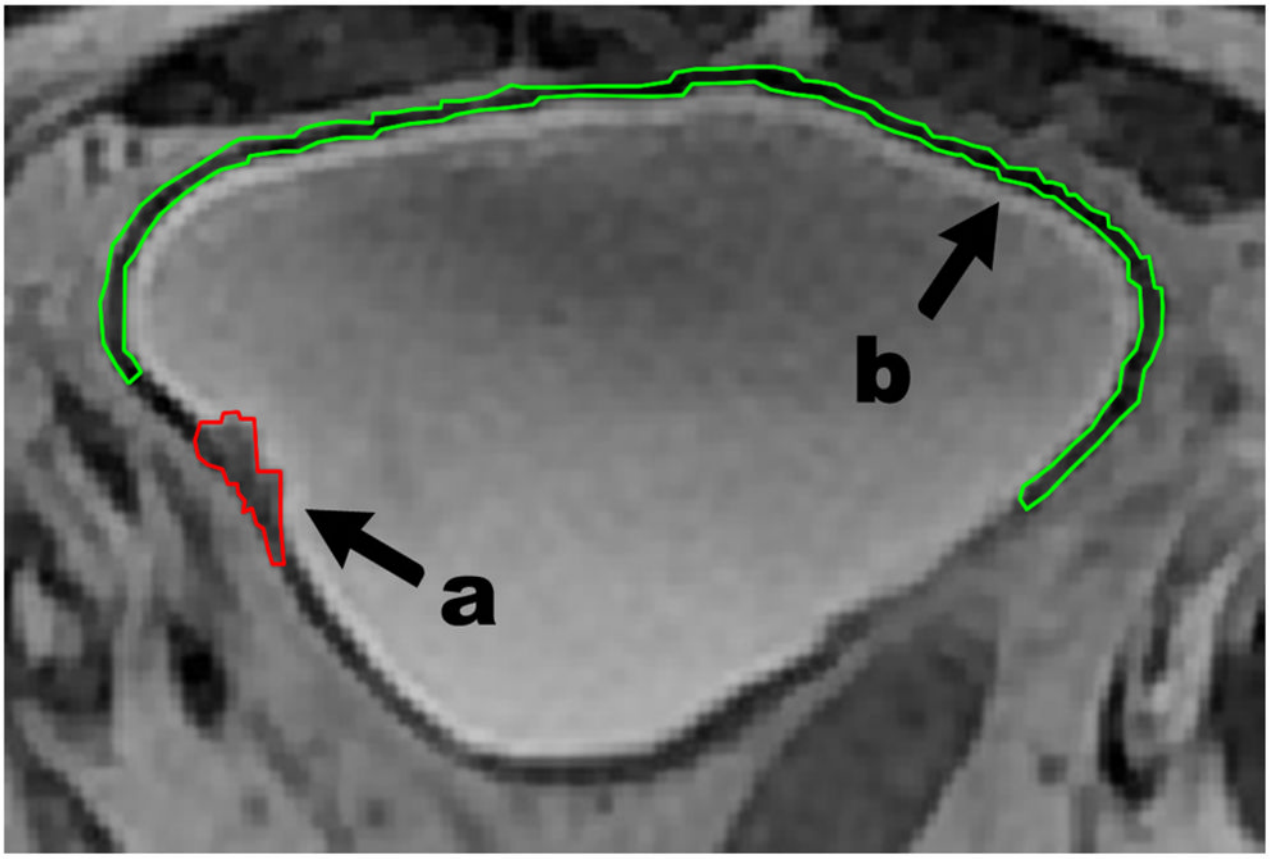

Figure 1.
Patient's magnetic resonance image with outlined regions of interest (ROIs). (a) ROI for carcinoma neoplasm; (b) ROI for bladder wall tissue.

TABLE 1A

The Textural Features Used in This Study (Simple Version)

Category	N	Features
Distribution of image gray level (9,10)	8	Mean, entropy, uniformity, SD, smoothness, skewness, Tm, kurtosis
Auto-covariance coefficient (12)	1	Norm of vector
Tamura features (13)	4	Contrast, directionality, line-likeness, regularity
Features derived from GLCM (14,15)	16	Sixteen features derived from the GLCM matrix, ie, f1: angular second moment, f2: contrast, f3: correlation, f4: sum of squares, f5: inverse difference moment, f6: sum average, f7: sum variance, f8: sum entropy, f9: entropy, f10: difference variance, f11: difference entropy, f12 and f13: information measures of correlation, f14: inertia, f15: cluster shade, and f16: cluster prominence.
Features derived from GLGCM (16)	11	Eleven features derived from the GLGCM matrix, ie, T1: small grads dominance, T2: big grads dominance, T3: gray asymmetry, T4: grads asymmetry, T5: energy, T6: correlation, T7: gray entropy, T8: grads entropy, T9: entropy. T10: inertia, and T11: DifferMoment.

TABLE 1B

The Textural Features Used in This Study (Version With Definitions)

Category	Features	Computation Formula	Notes
Distribution of image gray level (9,10)	Mean	$m=\frac{1}{n}\sum_{(x,y)\in R}[f(x,y)]$	$f(x,y)$ represents the intensity value of a pixel located at (x,y). n means the total number of pixels within the ROI, k means the number of gray level value within the ROI, and $p(I_i)$ means the probability of value I_i occurring in the ROI.
	Entropy	$e=-\sum_{i=1}^{k}[p(I_i)]\log_2[p(I_i)]$	
	Uniformity	$u=\sum_{i=1}^{k}[p(I_i)]^2$	
	Standard deviation	$s=\sqrt{\frac{1}{n-1}\sum_{i=1}^{n}[f_i(x,y)-m]^2}$	
	Smoothness	$R=1-\frac{1}{1+s^2}$	
	Skewness	$S=\frac{n}{(n-1)(n-2)s^3}\sum_{i=1}^{n}(I_i-m)^3$	
	Third moment (Tm)	$\mu_3=\sum_{i=1}^{k}(I_i-m)^3p(I_i)$	
	Kurtosis	$K=\frac{n(n+1)}{(n-1)(n-2)(n-3)s^4}\sum_{i=1}^{n}(I_i-m)^4-3\frac{(n-1)^2}{(n-2)(n-3)}$	
Auto-covariance coefficient (12)	Norm of vector (NOV)	$\mathrm{NOV}=\sqrt{\sum_{\Delta m=0,\Delta n=0}^{n}\gamma(\Delta m,\Delta n)^2}$, where $\gamma(\Delta m,\Delta n)=\frac{A(\Delta m,\Delta n)}{A(0,0)}$, $A(\Delta m,\Delta n)=\frac{1}{Count_{(\Delta m,\Delta n)}}\cdot\sum_{x0}^{M-1-\Delta m}\sum_{y=0}^{N-1-\Delta n}[f_{in}(x,y)-\bar{f}_{in}]\times[f_{in}(x+\Delta m,y+\Delta n)-\bar{f}_{in}]$	$f_{in}(x,y)$ and $f_{in}(x+\Delta m,y+\Delta_n)$ are gray levels of pixels (i,j) and $(i+\Delta m, j+\Delta n)$ inside a ROI of size $M \times N$. $\bar{f}_{in}$ is the mean value of all pixels and $\mathrm{Count}_{(\Delta m,\Delta n)}$ is the number of pixel pairs inside a ROI, with given distance (Δm,

Category	Features	Computation Formula	Notes
			Δn) along the x and y axes, respectively.
Tamura features (13)	Contrast	$F_{con} = \sigma/(a_4)^{1/4}$, where $a_4 = \mu_4/\sigma^4$	μ_4 is the 4th moment of all pixels about the mean inside a ROI, and σ^2 is the variance. θ is the gradient direction of a pixel, and $N_\theta(k)$ is the number of pixels with which $(2k-1)\pi/2n < \theta < (2k+1)\pi/2n$ and the gradient norm $\|G\| \geq t$ (a preset thresholding). $H_D(\varphi)$ can be regarded as the histogram of θ, where n_p is the number of peaks, φ_p is the position of the pth peak, and w_p is the range between peaks. P_{Dd} means the $m \times n$ local cooccurrence matrix with a given distance along a given direction. r is a normalizing factor and σ_{xxx} means the standard deviation of the feature F_{xxx}.
	Directionality	$H_D(k)=N_\theta(k)/\sum_{i=0}^{n-1} N_\theta(i) \quad k=0,1,\cdots,n-1$ $F_{dir}=\sum_p^{n_p}\sum_{\varphi\in w_p}(\varphi-\varphi_p)^2 H_D(\varphi)$	
	Line-likeness	$F_{lin}=\sum_i^n\sum_j^n P_{Dd}(i,j)\cos\left[(i-j)\frac{2\pi}{n}\right]/\sum_i^n\sum_j^n P_{Dd}(i,j)$	
	Regularity	$F_{reg} = 1 - r(\sigma_{crs} + \sigma_{con} + \sigma_{dir} + \sigma_{lin})$ $F_{crs}=\frac{1}{M\times N}\sum_{i=1}^{M}\sum_{j=1}^{N} S_{best}(i,j)$ where	
Features derived from GLCM (14,15)	f1–f16 derived from the GLCM matrix	$M_{d,\theta}(i,j)=\sum_{x=1}^{M}\sum_{y=1}^{N}\begin{cases}1 & if\ (x,y),\ (x',y')\varepsilon R^2, f(x,y)=i\ and\ f(x',y')=j\\ 0 & otherwise\end{cases}$ f1: angular second moment, f2: contrast, f3: correlation, f4: sum of squares, f5: inverse difference moment, f6: sum average, f7: sum variance, f8: sum entropy, f9: entropy, f10: difference variance, f11: difference entropy, f12 & f13: information measures of correlation, f14: inertia, f15: cluster shade, and f16: cluster prominence.	$I(x,y)$ represents the intensity value of a pixel located at (x,y). $M \times N$ is the size of the ROI. $M_{d,\theta}(i,j)$ is the (i, j) element of the GLCM matrix, representing the relative frequency with which two pixels with given gray levels of i and j are separated by a given pixel distance of d along the direction of θ.
Features derived from GLGCM (16)	T1–T11 derived from the GLGCM matrix	$M'(i,j)=\sum_{x=1}^{M}\sum_{y=1}^{N}\begin{cases}1 & \text{if}\ (x,y)\varepsilon R^2, \quad f(x,y)=i\ \text{and}\ f_g(x,y)=j\\ 0 & \text{otherwise}\end{cases}$ T1: small grads dominance, T2: big grads dominance, T3: gray asymmetry, T4: grads asymmetry, T5: energy, T6: correlation, T7: gray entropy, T8: grads entropy, T9: entropy. T10: inertia, and T11: DifferMoment.	$f_g(x,y)$ represents the gradient image of $I(x,y)$. $M'(i,j)$ is the (i, j) element of the GLGCM matrix, representing the

Category	Features	Computation Formula	Notes
			relative frequency with which a pixel with given gray level of *i* and gradient of *j* appeared in the ROI.

GLCM, gray level cooccurrence matrix; GLGCM, gray level-gradient co-occurrence matrix; grads, gradient; N, number of features; Tm, third moment.

TABLE 2

Histologic Subtypes and Staging of Patients

Subtype	Stage	Number	Age Range	Mean Age ± SD
Uc	T1	4	50–58	54.75 ± 3.59
Uc	T2	13	32–73	59.31 ± 12.10
Uc	T3	3	64–74	70.33 ± 5.50
Uc	T4	2	66	66.00 ± 0.00
	Total	22	32–74	60.59 ± 10.59

Uc, urothelial carcinoma.

Acad Radiol. Author manuscript; available in PMC 2013 September 01.

TABLE 3

t-test Results between Groups A and B ($N_a = 21$, $N_b = 20$)

Features	*P* (Two-Tailed)
Mean	.0000
Entropy	.0000
Uniformity	.0010
Standard deviation	.0000
Smoothness	.0000
Third movement	.0000
Norm	.0000
Contrast	.0000
Line_likeness	.0060
T1	.0000
T2	.0000
T3	.0000
T4	.0080
T5	.0010
T7	.0000
T8	.0098
T9	.0000
T10	.0000
T11	.0000
f1	.0000
f2	.0000
f3	.0000
f4	.0000
f5	.0000
f6	.0000
f7	.0000
f8	.0000
f9	.0000
f10	.0000
f11	.0000
f14	.0000
f15	.0000
f16	.0000

The difference between groups A and B was considered to be significant if $P < .01$.

TABLE 4

t-test Results between Groups B and C ($N_b = 20$, $N_c = 23$)

Features	*P* (Two-tailed)
Entropy	.0000
Uniformity	.0000
Directionality	.0050
T5	.0020
T6	.0010
T9	.0000
f1	.0000
f9	.0000
f12	.0070

The difference between groups B and C was considered to be significant if $P < .01$.

TABLE 5

Analysis of Variance between Groups B1 and C, B2 and C

Feature	B2 and C	*P*	B1 and C	*P*
Mean	△	.639	○	.733
Entropy	◢	.001	●	.005
Uniformity	◢	.003	●	.011
Standard deviation	◢	.044	○	.149
Smoothness	△	.079	○	.310
Third moment	△	.362	●	.025
Norm	△	.240	○	.120
Contrast	△	.138	○	.176
Line_likeness	◢	.002	○	.437
T1	△	.632	○	.469
T2	△	.810	○	.350
T3	◢	.041	○	.777
T4	◢	.017	○	.517
T5	◢	.007	●	.014
T7	◢	.042	○	.856
T8	◢	.021	○	.218
T9	◢	.000	●	.015
T10	△	.605	○	.967
T11	△	.756	○	.279
f1	◢	.000	●	.005
f2	△	.186	○	.814
f3	△	.931	○	.134
f4	△	.565	○	.453
f5	△	.085	○	.861
f6	△	.736	○	.681
f7	△	.603	○	.672
f8	◢	.007	○	.753
f9	◢	.000	●	.001
f10	◢	.032	○	.426
f11	◢	.028	○	.578
f14	△	.186	○	.814
f15	△	.940	○	.052
f16	△	.182	○	.103

◢significant difference between groups B2 and C; △, no significant difference between groups B2 and C; ●, significant difference between groups B1 and C; ○, no significant difference between groups B1 and C.

The difference between groups was considered to be significant if $P < .05$. Nine features show significant difference between subgroup B2 and group C and no significant difference between subgroup B1 and group C (indicated by ▲ and ○). Only one feature shows the opposite result (indicated by △ and ●).